Numerical study of continuous and discontinuous dynamical phase transitions for boundary-driven systems

Ohad Shpielberg,[1,2,*] Yaroslav Don,[2] and Eric Akkermans[2]
[1]*Laboratoire de Physique Théorique, École Normale Supérieure and CNRS, 75005 Paris, France*
[2]*Physics Department, Technion–Israel Institute of Technology, 3200003 Haifa, Israel*
(Received 5 January 2017; published 24 March 2017)

The existence and search for thermodynamic phase transitions is of unfading interest. In this paper, we present numerical evidence of dynamical phase transitions occurring in boundary-driven systems with a constrained integrated current. It is shown that certain models exhibit a discontinuous transition between two different density profiles and a continuous transition between a time-independent and a time-dependent profile. We also verified that the Kipnis-Marchioro-Presutti model exhibits no phase transitions in a range much larger than previously explored.

DOI: 10.1103/PhysRevE.95.032137

I. INTRODUCTION

Out-of-equilibrium systems are currently an object of considerable attention both in classical and quantum physics [1–8]. An important aspect of out-of-equilibrium physics resides in the study of nonequilibrium steady states of boundary-driven systems (e.g., two reservoirs at nonequal densities) and corresponding fluctuations about the steady state. A useful approach in the study of nonequilibrium steady states is a hydrodynamic description known as the macroscopic fluctuation theory (MFT) [9–11]. The MFT provides an efficient way to obtain an expression for the probability of observing steady-state fluctuations. As such, the MFT has proven useful in obtaining various properties such as out-of-equilibrium density fluctuations [12–14], Clausius inequality [15], the emergence of void formations [16], and others [17–22].

Another important problem in that field is the characterization of current fluctuations. Current fluctuations have been thoroughly studied in statistical physics [23–27] as well as in mesoscopic physics [28–30]. Knowledge of current fluctuations allows us to measure how close a fluctuation is to the steady state. Moreover, the noisy nature of the measurement allows us to obtain information about the system under study [31].

Current fluctuations can be obtained from the probability $P_t(Q)$ that a net amount of Q particles (or any other amount, e.g., heat) flowed through the system during a time t. Generally, $P_t(Q)$ is dominated by a single fluctuation. However, it is a difficult optimization problem [32]. It was conjectured in [33] that the dominant trajectory is time-independent. This is the content of the additivity principle (AP), which allows us to simplify the aforementioned minimization problem, and it has proven useful [8,24,32,34–36].

In certain cases, the AP solution may become nonunique, or overtaken by a time-dependent solution. Until recently [37], there were no known physical examples of a transition between AP solutions in boundary-driven systems. Moreover, as of yet there is no example of a continuous transition from an AP solution to a time-dependent one (namely, breaking of the AP assumption[1]). The possibility of discontinuous transitions was discussed in [32,38], and a mechanism for them was found in [37].

By analogy with thermodynamic phase transitions, it is useful to interpret a breaking of the AP assumption or a discontinuous transition as a dynamical phase transition (DPT) of first and second order, respectively, due to the nonanalyticity of $P_t(Q)$ at the transition point [34,38,39]. This interpretation has been used in [39] to obtain a sufficient and necessary condition for the validity of the AP for small fluctuations. Note that while one-dimensional equilibrium thermodynamic systems with short-range interactions never display phase transitions [40], constrained systems—in or out of equilibrium—may very well present them [25,41,42].

The purpose of this paper is to numerically implement the tools developed in [39] for some models of interest. First, we report a thorough numerical study of the Kipnis-Marchioro-Presutti (KMP) model [43], which shows that it never violates the sufficient and necessary conditions given in [39] and for a much broader parameter range than previously explored. Second, we present numerical evidence for either first- or second-order DPT as a function of the strength of a constrained current in some boundary-driven systems. A physical example for such a process is the long-range hopping with exclusion model proposed by Bodineau [44].

The outline of this paper is as follows. In Sec. II, we recapitulate briefly the MFT and the calculation of current fluctuations. The AP assumption—as presented in [33]—is outlined, and a sufficient and necessary condition for its validity is derived for continuous transitions, similarly to [39]. Section III reviews the models we probe numerically for DPTs. In Sec. IV, we show evidence for DPTs in two models, and we assert the absence of DPT in the KMP process for a broad range of currents in accordance with [34]. Section V summarizes our findings and presents further directions of study.

*ohad.shpielberg@lpt.ens.fr

[1]However, for periodic boundary conditions, many models were shown to break the AP assumption explicitly; see [25] and [41,42,49].

II. THEORETICAL BACKGROUND

We consider diffusive particles in a one-dimensional system of size L as described by the MFT (see [34,45] for a microscopic derivation). Particles can be injected to—or extracted from—the system at the boundaries only. This condition is expressed by the continuity equation

$$\partial_\tau \varrho(x,\tau) = -\partial_x j(x,\tau), \tag{1}$$

which relates the coarse-grained density $\varrho(x,\tau)$ and current density $j(x,\tau)$ by using rescaled coordinates for space $x \in [0,1]$ and time $\tau \in [0, t/L^2]$.

The MFT states that the probability to observe a fluctuation (ϱ, j) can be written using only the macroscopic diffusion coefficient D and conductivity σ, which generally depend on the local density ϱ. To define $D(\varrho)$ and $\sigma(\varrho)$, we consider a system coupled at each end to a reservoir with fixed densities ϱ_L and ϱ_R at $x = 0$ and 1, respectively. We take $\varrho_L = \varrho$ and $\varrho_R = \varrho + \Delta\varrho$ with $\Delta\varrho \ll 1$. The diffusion and conductivity are defined using the first two cumulant coefficients of the integrated number of particles Q,

$$J_s \equiv \frac{\langle Q\rangle}{t} = -\frac{1}{L}\, D(\varrho)\Delta\varrho, \tag{2a}$$

$$\frac{\langle Q^2\rangle_C}{t} = \frac{1}{L}\sigma(\varrho), \tag{2b}$$

where $\langle\cdot\rangle$ stands for an averaging with respect to the steady-state probability distribution, and $\langle Q^2\rangle_C \equiv \langle Q^2\rangle - \langle Q\rangle^2$.

The large deviation principle assumes that the probability to observe a net transfer of Q particles is given by

$$P_t(Q) \sim \exp[-t\,\Phi(J = Q/t)], \tag{3}$$

where J is the mean constrained current and $\Phi(J)$ is the large deviation function. Using the MFT, $\Phi(J)$ is expressed as a minimization problem [32,38,39]. Obtaining $\Phi(J)$ explicitly requires finding an optimal fluctuation (ϱ, j) that satisfies Eq. (1) and the mean constrained current $J = Q/t$.

Another useful representation of current statistics is obtained from the cumulant generating function $\mu(\lambda)$. Here, the two previous constraints are relaxed, the mean constrained current J is replaced by λ, and a Lagrange multiplier p is introduced to account for the continuity equation (1). The cumulant-generating function is the Legendre transform of the large deviation function, $\mu(\lambda) = \sup_J [\Phi(J) - \lambda J]$.

The cumulant-generating function is then explicitly written as a minimization problem [30,34,46],

$$\mu(\lambda) = -\frac{L}{t}\min_{\varrho,p}\int_0^1 dx \int_0^{\frac{t}{L^2}} d\tau\,(p\,\partial_\tau\varrho - \mathcal{H}), \tag{4}$$

where[2]

$$\mathcal{H} = -D(\varrho)\partial_x\varrho\,\partial_x p + \tfrac{1}{2}\sigma(\varrho)(\partial_x p)^2. \tag{5}$$

The trajectories (ϱ, p), which solve the minimization problem, satisfy Hamilton equations subjected to the boundary conditions [39]

$$\varrho(x=0,\tau) = \varrho_L, \quad \varrho(x=1,\tau) = \varrho_R, \tag{6a}$$

$$p(x=0,\tau) = 0, \quad p(x=1,\tau) = \lambda. \tag{6b}$$

Solving this problem proves generally difficult. In [33], it was conjectured (the AP assumption) that the optimal density profile is time-independent.[3] In this case, the AP assumption implies that $(\varrho_0(x), p_0(x))$ are solutions of

$$\partial_x(D_0\,\partial_x\varrho_0 - \sigma_0\,\partial_x p_0) = 0, \tag{7a}$$

$$-D_0\,\partial_{xx}p_0 - \tfrac{1}{2}\sigma_0'(\partial_x p_0)^2 = 0, \tag{7b}$$

where $\sigma'(\varrho) \equiv d\sigma/d\varrho$ and D_0, σ_0, σ_0' are evaluated at ϱ_0. According to (6), the boundary conditions for Eqs. (7) are

$$\varrho_0(x=0) = \varrho_L, \quad \varrho_0(x=1) = \varrho_R, \tag{8a}$$

$$p_0(x=0) = 0, \quad p_0(x=1) = \lambda. \tag{8b}$$

In [39], a sufficient and necessary condition has been derived, which verifies whether or not the AP solution is a locally minimal solution. It relies on showing that the AP solution is incorrect only if there is an allowed fluctuation $(\delta\varrho, \delta p)$ about the AP solution (ϱ_0, p_0) that gives a lower value to $\mu(\lambda)$ in Eq. (4) (this approach disregards first-order DPTs).[4] It was found that the AP assumption is not valid for $\mu(\bar\lambda)$ if and only if [39] (a) $\exists(\bar\omega, \bar\lambda)$ such that there exists a nontrivial solution to the equations

$$\begin{aligned} i\omega f_\omega = {} & \partial_x[D_0'(\partial_x\varrho_0)f_\omega + D_0(\partial_x f_\omega) \\ & - \sigma_0'(\partial_x p_0)f_\omega - \sigma_0(\partial_x g_\omega)], \end{aligned} \tag{9a}$$

$$\begin{aligned} i\omega g_\omega = {} & \big[-D_0'\,\partial_{xx}p_0 - \tfrac{1}{2}\sigma_0''(\partial_x p_0)^2\big]f_\omega - D_0(\partial_{xx}g_\omega) \\ & - \sigma_0'(\partial_x p_0)(\partial_x g_\omega); \end{aligned} \tag{9b}$$

(b) for these $(\bar\omega, \bar\lambda)$, $\delta s^2_{\bar\omega} < 0$, where

$$\delta s^2_\omega = \int dx \left[\frac{D_0'\sigma_0' - D_0\sigma_0''}{4D_0}(\partial_x p_0)^2|f_\omega|^2 + \frac{\sigma_0}{2}|\partial_x g_\omega|^2\right]. \tag{10}$$

Here $(f_\omega(x), g_\omega(x))$ are the Fourier modes of the fluctuations $(\delta\varrho, \delta p)$, namely $\delta\varrho = \sum_\omega f_\omega e^{i\omega\tau}$ and $\delta p = \sum_\omega g_\omega e^{i\omega\tau}$, and δs^2_ω is the Fourier transform of the variation of $\mu(\lambda)$ to second order in $\delta\varrho, \delta p$. The boundary conditions for (f_ω, g_ω) are

$$f_\omega(x=0) = f_\omega(x=1) = 0, \tag{11a}$$

$$g_\omega(x=0) = g_\omega(x=1) = 0, \tag{11b}$$

since the solutions $(\varrho_0 + \delta\varrho, p_0 + \delta p)$ must satisfy the boundary conditions (8).

Note that $f_\omega = g_\omega = 0$ is a trivial solution to the linear Eqs. (9). Clearly that trivial solution never corresponds to a

[2]Here we assume that the number of particles in the system is bounded.

[3]We will also consider p to be time-independent, although it may not necessarily be so.

[4]This scheme can only probe small fluctuations about the AP solution. To our knowledge, there are no sufficient and necessary conditions that accommodate large fluctuations.

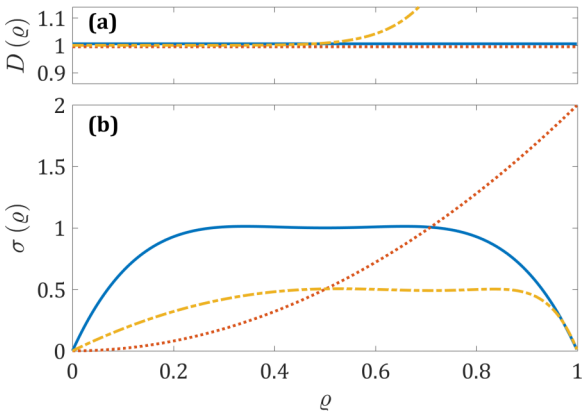

FIG. 1. (a) The diffusion D and (b) the conductivity σ. The models under inspection: in solid blue, the Mexican flat hat model for $A = 1$ and $B = -20$; in dotted red, the KMP model; in dashed yellow, the long-range hopping with exclusion model for $\alpha = 1/24$ and $\beta = 9$.

DPT as it yields $\delta s^2_\omega = 0$. Therefore, the main task of finding a numerical solution of Eqs. (9) is to force out that trivial solution and to find nontrivial ones.

We note that in [37], it was necessary to develop a nonlinear perturbation theory, namely to include higher-order terms, such as $\delta\varrho^2, \delta p^2, \delta\varrho\,\delta p$. However, it seems that the method presented in [37] cannot be extended to find time-dependent transitions. For the models considered here, linear perturbation theory is sufficient to observe DPTs.

There is no direct method to systematically search for first-order DPTs. However, one may encounter them while solving the AP equations (7) with boundary conditions (8). It happens when either the large deviation function $\Phi(J)$ or the cumulant-generating function $\mu(\lambda)$ favors one solution below some critical value and a second one above it (see Appendix B). There is no guarantee, however, that there is no third solution, which is always favorable.

III. MODELS

As of now, there is no known example of a process leading to a time-dependent second-order DPT under boundary drive. Note that from Eq. (10), one can infer a sufficient condition for the validity of the AP solution [39], namely

$$D_0'\sigma_0' \geqslant D_0\sigma_0''. \tag{12}$$

Several models, e.g., the symmetric simple exclusion process (SSEP) [23,33] and the zero-range process [32,33],[5] satisfy Eq. (12), so that the AP can be used to evaluate the cumulant-generating function.

Here we present three models (see Fig. 1) and discuss the occurrence of a DPT: (a) a toy model with three extremal points for $\sigma(\varrho)$, (b) the KMP model, and (c) the long-range hopping with exclusion model suggested by Bodineau [44]. We will analyze them numerically in the next section.

[5]Where it is assumed there is no accumulation of particles in the system. See [50] for an example in which this assumption does not hold.

A. A toy model—The Mexican flat hat

The first model we consider is built in an attempt to find a boundary-driven model that presents first- and second-order DPTs as well as being relatively simple to analyze numerically. The Mexican flat hat is not derived from any microscopic dynamics. We take $D(\varrho) = 1$ with $\sigma(\varrho) = A(\varrho - \frac{1}{2})^2 + B(\varrho - \frac{1}{2})^4 - \frac{A}{4} - \frac{B}{16}$, such that we may have a region in ϱ where the sufficient condition in Eq. (12) is not fulfilled. In that region, we look for a violation of the AP.

B. The KMP model

The KMP model [43] was the first model of heat transfer shown to satisfy Fourier's law, which is the counterpart of Fick's law for heat transfer.

In the KMP model, each site $i \in 1,\dots,L$ stores an energy $e_i \geqslant 0$. At each time step t, we choose two neighboring sites i and i'. They redistribute their respective energies according to a random value $p \in [0,1]$, namely $e_i(t+dt) = p\,e_i(t) + (1-p)e_{i'}(t)$ and $e_{i'}(t+dt) = (1-p)e_i(t) + p\,e_i'(t)$. This implies energy conservation at each time step, with fast equilibration between neighboring sites. The boundaries are considered as fictitious sites with energies drawn from a Boltzmann distribution of respective temperatures ϱ_l and ϱ_r.

Macroscopically, the KMP model is obtained by taking $D(\varrho) = 1$ and $\sigma(\varrho) = 2\varrho^2$ [43], where $\varrho(x,\tau)$ denotes the energy density instead of the particle density.

C. Long-range hopping with exclusion model

The long-range hopping with exclusion model proposed by Bodineau [44] is a one-dimensional lattice-gas model with L sites whose occupancy $n_i = \{0,1\}$ for $i \in 1,\dots,L$. A particle can hop from site i to a nearest-neighbor site $i \pm 1$ with rate 1 just like in the SSEP. Unlike SSEP, however, a particle is also allowed to hop from site i to site $i \pm (\beta+1)$ with a rate α provided that the β sites separating them are all occupied, as depicted below:

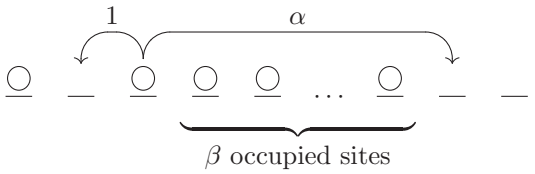

This model is a gradient model, a result that allows us to obtain D and σ analytically [47]. We obtain $D(\varrho) = 1 + \alpha(\beta+1)^2\varrho^\beta$ and $\sigma(\varrho) = 2\varrho(1-\varrho)D(\varrho)$ with $\varrho \in [0,1]$. This model allows some freedom in the form of D and σ due to the free parameters $1 \geqslant \alpha \geqslant 0$ and $\beta \in \mathbb{N}$.

IV. NUMERICAL METHOD—RESULTS

To probe for a second-order DPT, we solve Eqs. (7) and (9) with the boundary conditions (8) and (11).

A naive attempt to find a solution of Eqs. (9) using the numerical solution of Eqs. (7) will *almost always* yield the trivial solution $f_\omega = g_\omega = 0$ due to the linearity of the equations and their corresponding boundary conditions (11).

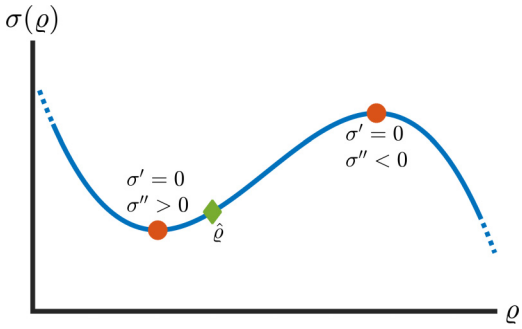

FIG. 2. Fixing the boundary conditions $\varrho_L = \varrho_R = \hat{\varrho}$ (green diamond) between a minimal and a maximal point in σ (red circles). For $D = 1$, we expect the AP density profile to increase as the current is increasing (see Appendix A for some insight). However, at some point the density profile reaches a maximal value of σ. Further heightening of the density profile is no longer favorable. This calls for a different characteristic solution of the density profile. It could conceivably be a different AP solution or a time-dependent solution.

We therefore employ a "sniping method": we condition the numerical solver to the boundary conditions,

$$f_\omega(x=0) = 0, \quad f_\omega(x=1) = 0, \tag{13a}$$

$$g_\omega(x=0) = 0, \quad \partial_x g_\omega(x=0) = 1, \tag{13b}$$

thus forcing the system away from the trivial solution. Note that due to the linearity of Eqs. (9), the particular choice of the value for the derivative condition, $\partial_x g_\omega(0) = 1$, changes the solution (f_ω, g_ω) only by a multiplicative factor, which is innocuous to the problem at hand. Generally, for a given (λ, ω) the solution of Eqs. (9) with the boundary conditions (13) does not satisfy the original boundary conditions (11). We identify a *proper* solution (f_ω, g_ω) only if $|g_\omega(1)| = 0$.

By changing the boundary conditions from (11) to (13), we find proper solutions by systematically scanning the (λ, ω) space. We then check the value of δs_ω^2. Only proper solutions with $\delta s_\omega^2 < 0$ indicate a second-order DPT.

We note that, given a solution at some λ_s, one must check that solutions also exist in a finite range around it. Otherwise, it is required to go beyond the linear perturbation theory considered here [37].

A. A toy model—The Mexican flat hat

The motivation behind this model is to lure the AP solution to follow a favorable path of the density profile due to a rapid increase of σ. This trend becomes unfavorable if the density profile hits a maximal point of σ (see Fig. 2 and Appendix A). To achieve that, we consider a model where σ has at least one minimum and one maximum, and we set $\varrho_L = \varrho_R = \hat{\varrho}$ such that $\hat{\varrho}$ lies between the two extreme points (see Fig. 2).

From the large deviation function picture (see Appendix A), one expects that increasing J (correspondingly, λ) manifests in an increase of the density profile, since σ is monotonously increasing initially for $\varrho > \hat{\varrho}$. However, for a sufficiently large current, the density profile reaches the maximal value in σ. Then, it is no longer beneficial to continue and increase the density profile. At this point a different solution, although not necessarily time-dependent, should take over.

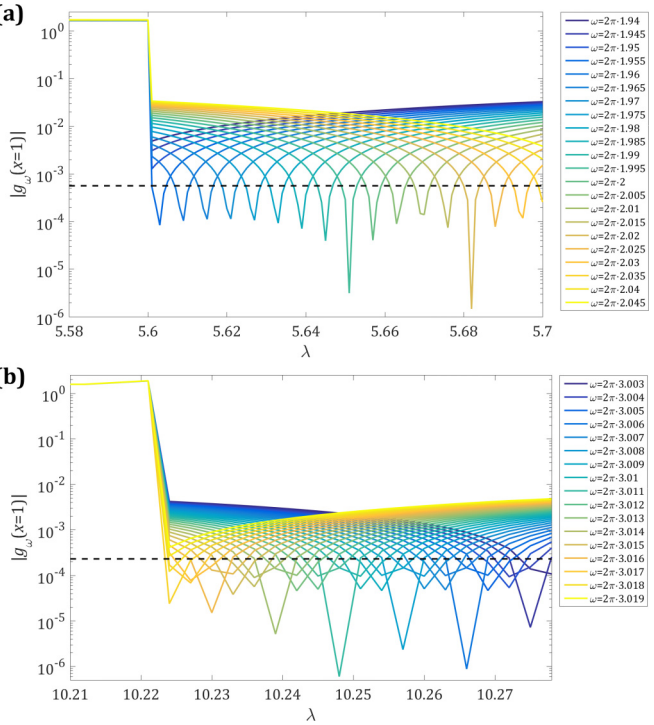

FIG. 3. The sniping method results for the Mexican flat hat and the long-range hopping with exclusion models. We are interested in finding a solution for which $|g_\omega(x=1)| = 0$ for some λ and ω using the sniping method. Identification of numerical zeros is made by going below the numerical error bars implying the existence of a solution to (9) with the boundary conditions (11). Solid lines: the absolute values of $g_\omega(x=1)$ using the sniping method. Dashed lines: the numerically estimated errors on $|g_\omega(x=1)|$. (a) The Mexican flat hat model for $A = 1$ and $B = -20$. (b) The long-range hopping with exclusion model for $\alpha = 1/24$ and $\beta = 9$. No solutions to (9) were found below $\lambda = 5.6$ in (a) and below $\lambda = 10.22$ in (b).

We find this behavior to be conceptually correct (see Appendix A for details). First, we notice a discontinuous transition between two AP solutions: a concave density profile and a convex density profile at λ_{c_1}. Namely, for $0 < \lambda < \lambda_{c_1}$ the concave density profile has a lower value for $\mu(\lambda)$ while for $\lambda_{c_1} < \lambda < \lambda_{c_2}$ the convex density profile is favorable. After which, at a higher λ_{c_2}, the convex density profile becomes unstable to small time-dependent fluctuations. We find this behavior for $\hat{\varrho} = 0.55$, with $\lambda_{c_1} \approx 3.70$ and $\lambda_{c_2} \approx 5.60$, which correspond to $J_{c_1} \approx 4.91$ and $J_{c_2} \approx 8.41$. For the second-order DPT at λ_{c_2}, there is a nonzero mode near $\omega_0 = 4\pi$ that allows nontrivial fluctuations (f_ω, g_ω) [see Fig. 3(a)]. This fluctuation was found to give a lower value than the AP solution for the cumulant-generating function $\mu(\lambda)$ as seen in Fig. 4(a). We note that this behavior can also be found for nonequal boundary conditions.

B. The KMP model

The KMP model was extensively studied numerically in the context of current fluctuations. For periodic boundary conditions, it was found that there exist such DPTs, and that for a certain λ the optimal solution becomes a traveling wave rather than a fixed density profile. However, for the boundary-driven

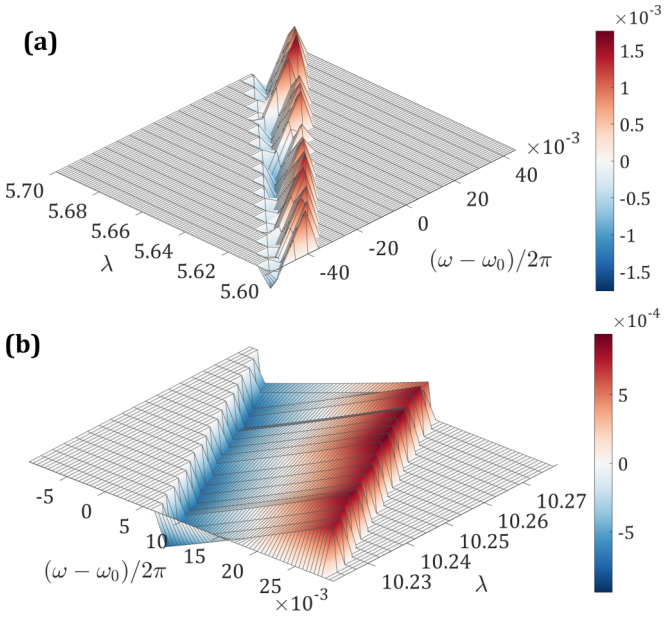

FIG. 4. The value of δs_ω^2 for a range of ω and λ above the critical region for the Mexican flat hat and the long-range hopping with exclusion models. Here, red and blue highlight the positive and negative values of δs_ω^2, respectively. The locations for which $\delta s_\omega^2 = 0$ imply that only the trivial solution $f_\omega = g_\omega = 0$ exists. The negative values of δs_ω^2 imply a second-order DPT. (a) The Mexican flat hat model for $\omega_0 = 4\pi$. (b) The long-range hopping with exclusion model for $\omega_0 = 6\pi$. The reference points ω_0 in (a) and (b) are chosen for aesthetic reasons.

case, there is no theoretical or numerical indication for such DPTs. In [35] the cumulant-generating function was probed for a range of values of λ using an exact simulation of the dynamics. For reservoir values of $\varrho_L = 2$ and $\varrho_R = 1$, they were able to verify the AP solution up to $\lambda \approx [-0.8, 0.45]$, which corresponds to the range $J \approx [-5.06, 13.9]$. Using the sniping method, we are able to verify that the AP solution is valid in the range $\lambda \approx [-0.9977, 0.49]$, which corresponds to $J \approx [-78.8, 30.6]$. This range is not the limit of our method, and it can be readily improved with further analysis. Note that for the above boundary conditions, $\lambda \in (-1, 0.5)$ corresponds to the whole range of current fluctuations. We find no nontrivial solutions to Eqs. (9) for these boundary conditions as well as for various others.

In summary, we were able to show that the AP solution is a minimum solution for very large currents—an order-of-magnitude improvement as compared to previous numerical results [35].

C. Long-range hopping with exclusion model

Contrary to the Mexican flat hat model, the long-range hopping with exclusion model is derived from a microscopic model. We produce an almost constant range of D by applying $\alpha = 1/24$ and $\beta = 9$, as shown in Fig. 1, and we get σ having three extremal points much in the spirit of the Mexican flat hat model. Probing for boundary conditions of $\varrho_L = \varrho_R = 0.75$, we find the same behavior as in the Mexican flat hat model, and with $\lambda_{c_1} \approx 5.01$ and $\lambda_{c_2} \approx 10.22$, which correspond to $J_{c_1} \approx 3.60$ and $J_{c_2} \approx 7.54$. At the continuous transition at λ_{c_2}, there is a nonzero mode near $\omega_0 = 6\pi$ that allows nontrivial fluctuations (f_ω, g_ω) [see Figs. 3(b) and 4(b)]. We note that the description of convex and concave solutions (see Appendix B) for this model is oversimplified due to the nontrivial $D(\varrho)$. Beyond λ_{c_1} the AP density profile can support more than one point at which $\frac{d\varrho}{dx} = 0$.

V. SUMMARY

We have presented evidence of two types of DPTs in the context of current fluctuations in boundary-driven systems. The first is a nonperturbative discontinuous transition between two different AP solutions, and the second is a continuous transition from an AP solution to a time-dependent solution. We have also numerically verified that the KMP model does not break the AP assumption under small perturbations up to high currents. It should be understood that a key ingredient in observing these DPTs is to set the boundary conditions such that the steady-state density profile is in the regime between two extreme values of the conductivity σ. We note that this scheme need not be unique, and it does not guarantee DPTs for general models. Moreover, continuous and discontinuous DPTs do not necessarily come in pairs.

One open question is to characterize the role the diffusion coefficient D plays in such a transition. We have also been unable to find a simple model for which the two types of DPTs can be analytically shown to occur. It is evident that there is a significant lack of understanding of the typical time-dependent density profile for boundary-driven processes, as opposed to periodic boundary conditions, where after the transition the density profile behaves like a traveling wave [41]. Moreover, it is of interest, although inherently difficult [48], to probe this transition in some experimental realization.

ACKNOWLEDGMENTS

This work has been supported by ANR-14-CE25-0003 and by Israel Science Foundation Grant No. 924/09. We would like to thank Yongjoo Baek for bringing to our attention his work, and Thierry Bodineau for suggesting his model. We acknowledge Kirone Mallick, Avi Aminov, and Vivien Lecomte for useful discussions.

APPENDIX A: THE LARGE DEVIATION FUNCTION FORMALISM

The purpose of this appendix is to present the large deviation function approach to current statistics, and to provide an intuitive approach to search for multiple AP solutions. The MFT provides a formal expression to the large deviation function [which is an alternative to the cumulant-generating function $\mu(\lambda)$],

$$\Phi(J) = \min_{\varrho, j \in \mathcal{A}_J} \frac{L}{t} \int dx\, d\tau\, \mathcal{L}(\varrho, j), \tag{A1}$$

where

$$\mathcal{L}(\varrho, j) = \frac{(j + D\partial_x \varrho)^2}{2\sigma}, \tag{A2}$$

such that $\varrho(x=0,\tau)=\varrho_L$, $\varrho(x=1,\tau)=\varrho_R$, and $\mathcal{A}_J$ is the set of all currents $j(x,\tau)$ such that $\int dx\,d\tau\; j(x,\tau)=Jt/L^2$. The AP assumption gives an upper bound $U(J)$ to $\Phi(J)$, where

$$U(J)=\frac{1}{L}\min_{\varrho(x)}\int dx\,\mathcal{L}_J[\varrho(x)] \tag{A3}$$

with $\mathcal{L}_J=\frac{(J+D\partial_x\varrho)^2}{2\sigma}$, $\varrho(x=0)=\varrho_L$, and $\varrho(x=1)=\varrho_R$. Finding the optimal solution $\varrho_0(x)$ boils down to solving an Euler-Lagrange equation $\frac{\delta\mathcal{L}_J}{\delta\varrho}=\frac{d}{dx}\frac{\delta\mathcal{L}_J}{\delta\partial_x\varrho}$, which yields

$$\partial_{xx}\varrho_0+(\partial_x\varrho_0)^2\left(\frac{D_0'}{D_0}-\frac{\sigma_0'}{2\sigma_0}\right)+J^2\frac{\sigma_0'}{2D_0^2\sigma_0}=0. \tag{A4}$$

It is clear that the AP density profile solution is indifferent to the sign of J, although $U(J)\neq U(-J)$ for $\varrho_L\neq\varrho_R$.

Now, after presenting the large deviation function formalism, it is possible to understand the logic behind searching for DPTs in the scenarios depicted in Fig. 2. For $\varrho_L=\varrho_R=\hat{\varrho}$ at $J=0$, the AP solution yields $\varrho_0(x)=\hat{\varrho}$. However, as we increase J, it is favorable to increase $\varrho_0(x)$ above $\hat{\varrho}$ as σ_0, the denominator of U, increases as well. However, for a large enough J, the density profile reaches the maximal point of σ, as depicted in Fig. 2. Therefore, the density going above this point decreases σ, and it will not be an optimal solution. We thus expect a change of trend in the optimal solution, where it can be a different AP solution or result in a transition to a time-dependent solution. We are unable to provide analytic proof for the transition or even an analytic estimation of the critical J, where we expect it to occur. However, the numerical solution for the AP corresponds to the prediction that there is a transition.

APPENDIX B: DETECTING FIRST-ORDER TRANSITIONS

In the main text, we report a discontinuous DPT for the Mexican flat hat and the long-range hopping with exclusion models. However, the numerical method described there is designed to systematically search for *continuous* DPTs. The discontinuous DPTs were found as a byproduct of this examination. They were observed in the following way.

The implementation of the method utilizes a numerical solver, which searches for a solution for the AP Eqs. (7). However, there is no guarantee that Eqs. (7) have a *single* solution. In the case of multiple solutions, the solver converges to one of them in an unpredictable way (depending on the initial guess, λ value, and boundary conditions). In other words, the solver has no preference to choose the optimal solution; it only finds saddle point (AP) solutions. Yet, the existence of multiple AP solutions may lead to a discontinuous DPT.

Using the main text method, the fingerprints of such a discontinuous DPT between different AP solutions are as follows: (a) an observation of a second spatially distinct solution in adjacent λ values, and (b) an identification of an overtaking of the cumulant-generating function corresponding to the first solution by the cumulant-generating function corresponding to the second solution in some finite interval of λ (similarly to the large deviation function depicted in Fig. 7). This provides a clear indication of a discontinuous DPT. However, this method is unreliable in evaluating the cumulant-generating function around the transition, or in obtaining the value of the transition; it can only suggest the general vicinity of the transition.

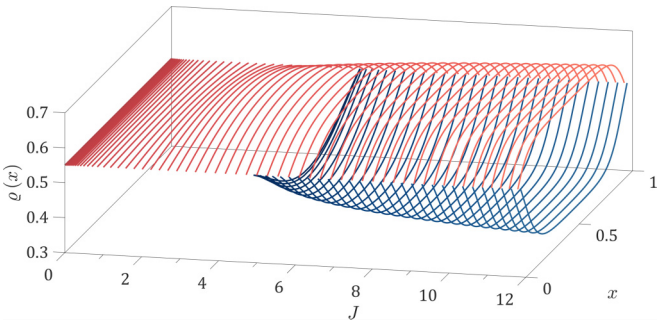

FIG. 5. The trajectories of the density profile $\varrho(x)$ for different values of J. Red (light gray) indicates the frowning solutions, and blue (dark gray) indicates the smiling solutions.

To properly describe a transition, we must procure its value and calculate the cumulant-generating function around it. To achieve these two purposes and to have a "sanity check" of the transition, we present below a different numerical approach. This approach relies heavily on insights from [33].

It is possible to show that Eq. (A4) can be reduced to a nonlinear first-order equation,

$$D^2(\varrho)\left(\frac{d\varrho}{dx}\right)^2=J^2[1+2K\sigma(\varrho)], \tag{B1}$$

where K is a constant determined by the boundary conditions. For equal boundary conditions $\varrho_L=\varrho_R=\hat{\varrho}$ such that $\sigma'(\hat{\varrho})\neq 0$, the density profile is never monotonous, except for $J=0$, where the solution is flat, namely $\varrho_0(x)=\hat{\varrho}$. Since it is not monotonous, there is at least one point for which $\frac{d\varrho}{dx}=0$ for differentiable density profiles. It makes sense to consider only a symmetric solution about $x\mapsto 1-x$. We assume that there is exactly one extreme point in the density profile for any $J\neq 0$, relying on the numerical results obtained by solving Eqs. (7) and (8) (see Fig. 5).

The density profile trajectory is analyzed as follows. Since the density profile is nonmonotonous, and from (B1), we find that $K\in[-1/2\sigma_{\max},-1/2\sigma(\hat{\varrho})]$, where $\sigma_{\max}$ is the maximal value σ can reach. For a given K in this range, one can find $\varrho^\star$, the value at which the density profile gradient vanishes at $x=1/2$, by using (B1) to obtain $\sigma(\varrho^\star)\leqslant-\frac{1}{2K}$. Here one can consider $-\frac{1}{2K}$ playing the role of a total energy, $\sigma(\varrho)$ being the potential, and ϱ the position. Therefore, one can deduce from this picture the possible density profiles for each K (see Fig. 6). Since σ is a nonmonotonous function, much like for a potential picture, there is some degeneracy in the value of $\varrho^\star$. For each K, there are two values for $\varrho^\star$, each corresponding to a different density profile. For $\varrho^\star>\hat{\varrho}$, the density profile is monotonously increasing in $x\in[0,1/2)$ and decreasing in $x\in(1/2,1]$, thus being designated the "frowning" solution. For $\varrho^\star<\hat{\varrho}$ instead, the density profile is monotonously decreasing within $x\in[0,1/2)$ and increasing within $x\in(1/2,1]$, thus being designated the "smiling" solution (see Fig. 5).

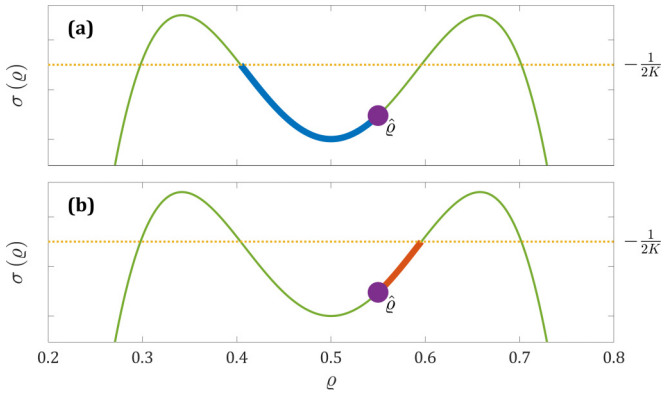

FIG. 6. The trajectory of the calculation of J. The green thin line is the conductivity profile σ, which plays the part of a potential. The yellow dotted line is the "total energy" $-\frac{1}{2K}$. The purple dot represents the boundary value $\varrho_L = \varrho_R = \hat{\varrho}$. (a) The trajectory for the smiling solution (in thick blue). (b) The trajectory for the frowning solution (in thick red).

Since the sign of the density profile gradient is fixed for $x \in [0,1/2)$, we can take the square root of (B1) and obtain

$$\frac{d\varrho}{dx} = \pm\frac{|J|}{D(\varrho)}\sqrt{[1+2K\sigma(\varrho)]}, \tag{B2}$$

with plus or minus for the frowning or smiling solutions, correspondingly (note that the solution is indifferent to the sign of J). From (B2), one can obtain an integral expression to the current

$$|J| = \pm 2\int_{\varrho^\star}^{\hat{\varrho}} d\varrho\, \frac{D(\varrho)}{\sqrt{1+2K\sigma(\varrho)}}, \tag{B3}$$

with again plus or minus for the frowning or smiling solutions, correspondingly. The choice of the $\pm$ sign depends on the $\varrho^\star \gtrless \hat{\varrho}$ case.

Using the density profile gradient of Eq. (B2) and the value of the current in Eq. (B3), we can find the expression for the large deviation function,

$$\Phi_\pm(J) = \pm 2\int_{\varrho^\star}^{\hat{\varrho}} d\varrho\, \frac{D(\varrho)}{\sigma(\varrho)}\left[1 - \frac{1+K\sigma(\varrho)}{\sqrt{1+2K\sigma(\varrho)}}\right], \tag{B4}$$

where, again, plus or minus corresponds for the frowning or smiling solutions. Solving numerically and comparing the two AP solutions for the Mexican flat hat (see Fig. 7), we observe that for $\hat{\varrho} = 0.55$ and for $A = 1, B = -20$, there is a single solution (frowning) for low currents, as expected. For higher currents where the two solutions exist, the smiling solution is favorable and marks the onset of a first-order DPT as the two solutions are not equal at the transition.

We find that the solution of this method corresponds to the behavior of the density profiles produced with the previous numerical approach, i.e., solving directly the AP Eqs. (7). The plot of $\Phi_\pm(J)$ for the long-range hopping with exclusion process is qualitatively the same as in the Mexican flat hat model given in Fig. 7, and thus it is not included here. We used this method to evaluate λ_{c_1} of the main text for both of these models.

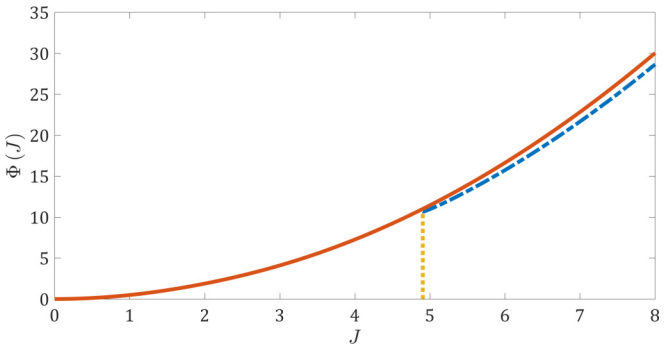

FIG. 7. The large deviation function $\Phi(J)$ corresponding to the two solutions of $\varrho(x)$ of Eq. (B1). The solid red line depicts solutions with $\frac{d\varrho}{dx} > 0$ at $x = 0$ (the frowning solution). The dashed blue line depicts solutions with $\frac{d\varrho}{dx} < 0$ at $x = 0$ (the smiling solution). Note that the smiling solution is attainable only from $J_{\text{transition}} \simeq 4.906$, where it is the favorable solution. The transition is indicated by the dotted yellow line.

[1] K. Mallick, Physica A **418**, 17 (2015).
[2] D. Bernard and B. Doyon, J. Stat. Mech.: Theor. Exp. (2016) 064005.
[3] S. Pilgram, A. N. Jordan, E. V. Sukhorukov, and M. Büttiker, Phys. Rev. Lett. **90**, 206801 (2003).
[4] C. Karrasch, R. Ilan, and J. E. Moore, Phys. Rev. B **88**, 195129 (2013).
[5] J. J. Mendoza-Arenas, S. Al-Assam, S. R. Clark, and D. Jaksch, J. Stat. Mech.: Theor. Exp. (2013) P07007.
[6] T. Prosen and M. Žnidarič, J. Stat. Mech.: Theor. Exp. (2009) P02035.
[7] X. Zotos, F. Naef, and P. Prelovšek, Phys. Rev. B **55**, 11029 (1997).
[8] K. Saito and A. Dhar, Phys. Rev. E **83**, 041121 (2011).
[9] L. Bertini, A. De Sole, D. Gabrielli, G. Jona-Lasinio, and C. Landim, Rev. Mod. Phys. **87**, 593 (2015).
[10] L. Bertini, A. De Sole, D. Gabrielli, G. Jona-Lasinio, and C. Landim, J. Stat. Phys. **135**, 857 (2009).
[11] L. Bertini, A. De Sole, and D. Gabrielli, Math. Phys. Anal. Geom. **6**, 231 (2003).
[12] L. Bertini, A. De Sole, D. Gabrielli, G. Jona-Lasinio, and C. Landim, J. Stat. Mech.: Theor. Exp. (2007) P07014.
[13] A. Aminov, G. Bunin, and Y. Kafri, J. Stat. Mech.: Theor. Exp. (2014) P08017.
[14] Y. Baek and Y. Kafri, J. Stat. Mech.: Theor. Exp. (2015) P08026.
[15] L. Bertini, D. Gabrielli, G. Jona-Lasinio, and C. Landim, Phys. Rev. Lett. **110**, 020601 (2013).
[16] P. L. Krapivsky, B. Meerson, and P. V. Sasorov, J. Stat. Mech.: Theor. Exp. (2012) P12014.
[17] E. Akkermans, T. Bodineau, B. Derrida, and O. Shpielberg, Europhys. Lett. **103**, 20001 (2013).

[18] T. Bodineau, B. Derrida, and J. L. Lebowitz, J. Stat. Phys. **140**, 648 (2010).
[19] T. Bodineau, B. Derrida, and J. L. Lebowitz, J. Stat. Phys. **131**, 821 (2008).
[20] T. Bodineau and M. Lagouge, J. Stat. Phys. **139**, 201 (2010).
[21] T. Agranov, B. Meerson, and A. Vilenkin, Phys. Rev. E **93**, 012136 (2016).
[22] P. L. Krapivsky, K. Mallick, and T. Sadhu, Phys. Rev. Lett. **113**, 078101 (2014).
[23] B. Derrida, B. Douçot, and P.-E. Roche, J. Stat. Phys. **115**, 717 (2004).
[24] M. Gorissen and C. Vanderzande, Phys. Rev. E **86**, 051114 (2012).
[25] C. Appert-Rolland, B. Derrida, V. Lecomte, and F. van Wijland, Phys. Rev. E **78**, 021122 (2008).
[26] N. Tizón-Escamilla, P. I. Hurtado, and P. L. Garrido, Phys. Rev. E **95**, 032119 (2017).
[27] N. Tizón-Escamilla, P. I. Hurtado, and P. L. Garrido, arXiv:1606.07507.
[28] E. Akkermans and G. Montambaux, *Mesoscopic Physics of Electrons and Photons* (Cambridge University Press, Cambridge, 2007).
[29] A. Kamenev, *Field Theory of Non-Equilibrium Systems* (Cambridge University Press, Cambridge, 2011).
[30] A. N. Jordan, E. V. Sukhorukov, and S. Pilgram, J. Math. Phys. **45**, 4386 (2004).
[31] D. Kambly, C. Flindt, and M. Büttiker, Phys. Rev. B **83**, 075432 (2011).
[32] L. Bertini, A. De Sole, D. Gabrielli, G. Jona-Lasinio, and C. Landim, J. Stat. Phys. **123**, 237 (2006).
[33] T. Bodineau and B. Derrida, Phys. Rev. Lett. **92**, 180601 (2004).
[34] A. Imparato, V. Lecomte, and F. van Wijland, Phys. Rev. E **80**, 011131 (2009).
[35] P. I. Hurtado and P. L. Garrido, Phys. Rev. Lett. **102**, 250601 (2009).
[36] P. I. Hurtado and P. L. Garrido, Phys. Rev. E **81**, 041102 (2010).
[37] Y. Baek, Y. Kafri, and V. Lecomte, Phys. Rev. Lett. **118**, 030604 (2017).
[38] L. Bertini, A. De Sole, D. Gabrielli, G. Jona-Lasinio, and C. Landim, Phys. Rev. Lett. **94**, 030601 (2005).
[39] O. Shpielberg and E. Akkermans, Phys. Rev. Lett. **116**, 240603 (2016).
[40] L. D. Landau, E. M. Lifshitz, and L. P. Pitaevskii, *Statistical Physics, Part 1*, Course of Theoretical Physics Vol. 5 (Pergamon, Oxford, 1980).
[41] L. Zarfaty and B. Meerson, J. Stat. Mech.: Theor. Exp. (2016) 033304.
[42] T. Bodineau and B. Derrida, Phys. Rev. E **72**, 066110 (2005).
[43] C. Kipnis, C. Marchioro, and E. Presutti, J. Stat. Phys. **27**, 65 (1982).
[44] T. Bodineau (private communication).
[45] B. Derrida, J. Stat. Mech.: Theor. Exp. (2007) P07023.
[46] J. Tailleur, J. Kurchan, and V. Lecomte, Phys. Rev. Lett. **99**, 150602 (2007).
[47] H. Spohn, Equilibrium fluctuations, *Large Scale Dynamics of Interacting Particles*, Texts and Monographs in Physics (Springer, Berlin, 1991), Pt. II, Chap. 2, pp. 175–211.
[48] N. Garnier and S. Ciliberto, Phys. Rev. E **71**, 060101 (2005).
[49] P. I. Hurtado and P. L. Garrido, Phys. Rev. Lett. **107**, 180601 (2011).
[50] O. Hirschberg, D. Mukamel, and G. M. Schütz, J. Stat. Mech.: Theor. Exp. (2015) P11023.